Gap Effect of a Rim Driven Thruster in Convergent and Divergent Duct Configuration

Marco Lugaresi, Diego Villa and Stefano Gaggero
University of Genoa, Genoa, Italy

1 Introduction

In the last years, due to the increase in maritime trade, the size of the ships and consequentially the power required has increased, highlighting the scalability problems of traditional shaft lines. In fact, as their size increases, the global ship efficiency, understood not directly as hydrodynamic efficiency but as system efficiency including loss of space on board, non-linear increase in weight and all the effects that contribute to reducing the performance of the ship in carrying out its mission, is reduced and greater design and construction difficulties and costs arise (Su et al. (2020)). In this context and thanks to important technological developments in the field of materials, electric propulsion and 3D printing, the rim driven thruster (RDT) gains more and more research interest for the use in naval propulsion. Initially proposed by Kort (1940), the RDT is a type of integrated engine propeller, also known as a shaftless propeller, in which the driving torque of the blades is given by a structural circular ring (rim) connected to the tip of the blades, in opposition to traditional propellers which are driven through the shaft (Grümmer (2016)). The configuration of the RDT fits very well with an electric motor. The stator can be contained inside the duct while the permanent magnet rotor can be included inside the rim. The main advantages of the RTD can be summarized in: it does not require watertight hull passages for rotating elements, being completely immersed in water it does not require dedicated cooling systems, it has a compact design which reduces overall dimensions and weight on board, it has no mechanical performance losses due to power transmission in the shaft line, the environmental impact due to radiated noise is significantly reduced both due to the use of the electric motor and to the absence of tip vortex thanks to the presence of the rim (Gaggero (2020)). Structurally, the RDT resembles a ducted propeller, however, unlike the latter, the RDT does not have tip clearance since the blades are structurally connected to the rim. Instead a gap clearance exists between the rim and the duct. This difference generates significant variations in the flow field and in the fluid phenomena involved, causing remarkable differences in the open water performance and in the flow characteristics. In recent years, several studies have been conducted on RDTs and significant progress has been made especially in improving electromagnetic performance, decreasing weight and bearings. Several works have also focused on the hydrodynamic efficiency which is influenced by several factors including the blade structure, the shape and size of the shroud and the gap characteristics (Yan et al. (2017)). The first studies on RDT were conducted using potential methods and in particular lifting line based panel codes (Pashias and Turnock. (2003)). Another approach proposed by Kinnas et al. (2009) used potential methods combining the lifting surface with a boundary element method. In particular, a mixture of lifting surface and RANS equations is used to calculate the effective wake at each iteration which is then used as input for the BEM method allowing the performance to be calculated. More recent studies have shown that, although the computational efficiency of potential methods makes them attractive for geometry selection and design, they are not suitable for correctly predicting the performance of an RDT. Song et al. (2015) conducted a comparative analysis between RDTs with and without axis concluding that the absence of the axis improves efficiency by up to 2%. The presence of the hub in fact causes an axial acceleration of the fluid which reduces the angle of attack radially along the blade and also induces greater vorticity which causes a greater loss of energy. Cao et al. (2012) investigated through RANS simulations the radial and the along-chord distribution in different RDT configurations, identifying the presence of combined root vortices and the formation of tip vortexes at a certain distance from the propeller disk. Dubas et al. (2015) conducted an analysis comparing stationary and unsteady simulations for the prediction of rotor-stator interaction and testing different turbulence models, concluding that the k-ω SST model is the most suitable for RDT simulations at low advance coefficients. Lea et al. (2003) through experiments on commercial RDTs have highlighted that, compared to ducted propellers, RDT have a higher tip load and less cavitation, effects which can be attributed to the presence of the rim. Liu et al. (2022) conducted simulations on RDTs with different shroud geometries presenting the results in terms of efficiency and flow field to better understand the effects of duct on propeller performance.

In general, the experimental works of Hughes et al. (2000) and Abu Sharkh et al. (2001) highlighted that the hydrodynamic efficiency of RDTs is lower with respect of ducted propellers, in fact the efficiency of RDTs is generally lower than 0.5 (Liu and Vanierschot (2021), Jiang et al. (2022), Liu et al. (2023)). This result, however, is partly attributable to the fact that the geometries typically used for RDTs are not designed ad hoc but derive from well known ducted propellers shapes. In fact, as highlighted by Peng et al. (2023) little RDT geometry data is available that can be freely used for academic research and, for this reason, as also highlighted in Liu and Vanierschot (2021) combinations of Ka4-70 propellers and MARIN 19A or MARIN 37 duct are often used. Moreover, most studies on the efficiency of RDTs have focused on the performance of the duct and propeller but the influence of the gap also plays an important role. In fact, the analysis conducted in Liu and Vanierschot (2021) highlight that the gap has a negative influence on RDT performance, leading this type of thruster to be less efficient when compared to ducted propellers. Cao et al. (2014) analyzed the effect of the radial and axial dimensions of the gap with and without a propeller, the results show that widening the gap increases the torque needed to move the propeller. The same result is confirmed by the study by Lin et al. (2023) which achieves this result increasing the front and rear side angle of the rim in order to reduce its width. Furthermore, they propose an empirical formula to estimate the torque increase which however has very limited application since the effect not only depends on the characteristics of the gap but also on the pressure field and therefore on the shape of the duct and of the propeller. Is also important to note that the literature currently available is related to accelerating (or converging) duct geometries which have the purpose of increasing the thrust of the RDT by accelerating the flow. However, in applications where the focus is on the cavitation reduction, the duct can be of a divergent type with the aim of increasing the pressure upstream of the rotor.

In this study, the effect of the gap on a convergent and a divergent duct RDT is analyzed. The geometries of propellers and ducts came from the work of Gaggero (2020) which implements a RDT design based on RANS simulations and optimization via genetic algorithm. On these geometries, the fluid dynamic fields were analyzed both with and without the gap geometrically resolved. Morover a parametric study on the gap shape is conducted applying some changes in shape and in the operating conditions. Section 2 presents the geometries used, the governing equations, the modeling hypotheses, the mesh, the boundary conditions and the numerical method used in the study. In section 3 the results obtained are presented and discussed. Finally, in section 4 we draw conclusions and indicate some recommendations for future work.

2 Numerical simulation methodology

2.1 Geometries description

The RDT geometries used in this article are obtained from the works of Gaggero (2020), Gaggero (2020b) and Gaggero et al. (2013). The geometry of rim driven configuration with decelerating duct (DRD), shown in figure 1a, is made up of the six blades propeller (z6-4097) obtained in Gaggero (2020) associated with the divergent nozzle of the ducted propeller reference presented in Gaggero et al. (2013). This geometry was designed to avoid the inception of cavitation as much as possible and, in fact, the purpose of the divergent duct is to increase the pressure upstream of the propeller. The propeller obtained is, thanks to the optimization process, designed specifically to work in the flow conditions of the associated duct at the selected design condition.

The geometry of the rim driven configuration with accelerating duct (CRD), shown in figure 1b, is taken from Gaggero (2020b) and is made up of a convergent duct (19A) designed to axially accelerate the flow, contributing to the thrust especially in bollard pull conditions, combined with a 5-blades propeller, specifically designed to work in the flow conditions generated by the duct.

Both RDT geometries are obtained on the basis of RANS simulations performed on a geometry

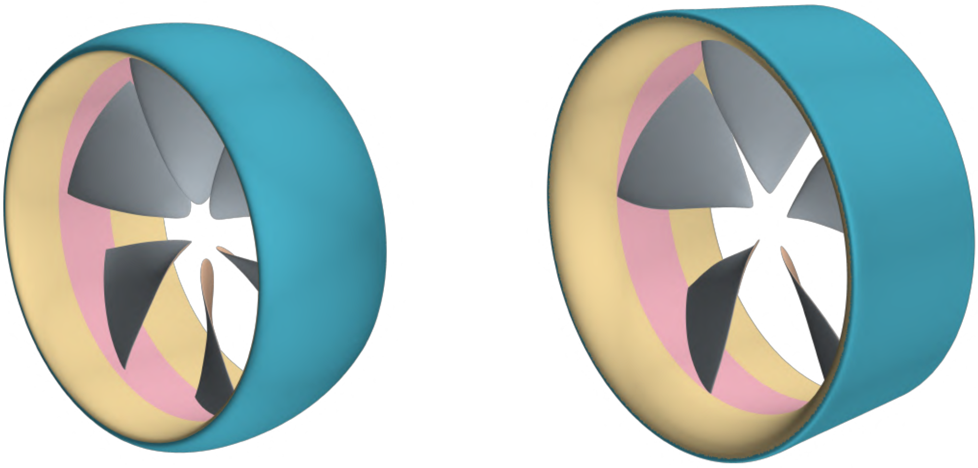

(a) (b)

Fig. 1: DRD (a) and CRD (b) geometries without geometrically resolved gap.

which, as visible in figure 1, does not explicitly contain the geometry of the gap. The rim is in fact modeled as a portion of the internal duct surface that extends axially from just before the propeller to shortly after. This choice, which has the aim of limiting computational costs can be accepted in a relative comparison based, quite demanding, design process but become a limit in correctly determining the absolute performance of the RDT considered. In fact, as highlighted by various works including for example Liu and Vanierschot (2021), the effect of the gap is not negligible and can lead to a loss of efficiency up to 2%. To investigate this aspect on above introduced optimized RDT, the geometries shown in figures 2 were produced.

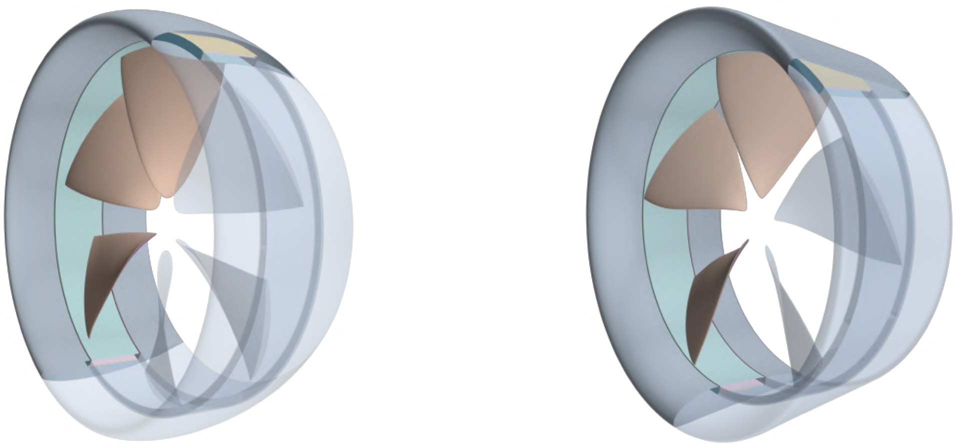

(a) (b)

Fig. 2: DRD (a) and CRD (b) geometries with geometrically resolved gap.

In these geometries the gap is built using the same parametric philosophy illustrated in figure 3 where the gap geometry is obtained using the parameters listed in table 1.

Table 1: Example of gap geometry parameters

ID	w [mm]	d [mm]	t [mm]	α_1 [°]	α_2 [°]
15/-45	40	5	1	15	-45

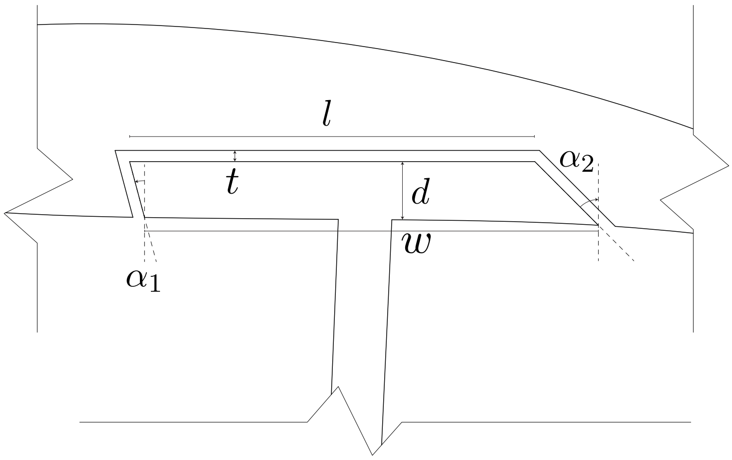

Fig. 3: Gap geometrical description.

Keeping constant w and d, the geometric characteristics of the gap were then varied parametrically in terms of:

1. gap thickness (t) with the values: [0.1, 0.3, 0.5, 0.8, 1.0, 1.2, 1.5] mm
2. front angle of the gap (α_1) with the values from -60° to 60°, step 15°
3. rear angle of the gap (α_2) with the values from -60° to 60°, step 15°

to better understand which characteristics, in addition to the width of the gap already highlighted by various works, had an impact on the performance of the RDT and how the gap affects the efficiency in both DRD and CRD configurations of thruster and considering the geometry of duct and propeller.

2.2 Simulations set-up

Most calculations were carried out using RANS for a single-phase fluid and incompressible flow. Star-CCM+ (Siemens (2021)) was used as solver on an unstructured mesh made of polyhedra using the Finite Volume method and second order discretization schemes for all the physical quantities. By using a Moving Reference Frame and by exploiting the periodicity of the problem, only one blade passage is considered in the stationary analyses while local mesh refinements account for the propeller and the duct wake. The computational domain, shown in figure 4 has a cross area at the propeller plane one hundred times higher than the area of the propeller disk (D_{domain}/D_{prop} = 10), the inlet is placed four propeller diameters in front of the propeller, the outlet six propeller diameters aft, and uniform inflow is assumed as the initial condition.

The k-ω SST turbulence model is used to compute the turbulent viscosity in a simulation where the turbulence intensity is set equal to 1% and the turbulent to molecular viscosity ratio is equal to 10.
To validate the assumptions made using stationary analyzes and exploiting the symmetry of the problem, unsteady simulation of the gap resolved reference RDTs were carried out. In these, the basic assumptions of the modeling and the mesh parameters are the same as in the stationary analysis with the following differences:

- the calculation domain is a full cylinder with diameter 10 D_{prop}, containing all the propeller blades so the number of cells is about $Z \cdot n_{steady}$ where Z is the number of blades and n_{steady} is the number of cells in steady state simulations,
- the geometries of the rim and propeller blades are inserted in a small cylindrical domain actually rotating thanks to the movement of the mesh,
- the second order time-marching scheme use a time step set to have a rotation of 1° per time-step, the stopping criteria are set to simulate at least 5 complete revolutions of the propeller and with a convergence of 1% in the average thrust of the last revolution compared to the previous one.

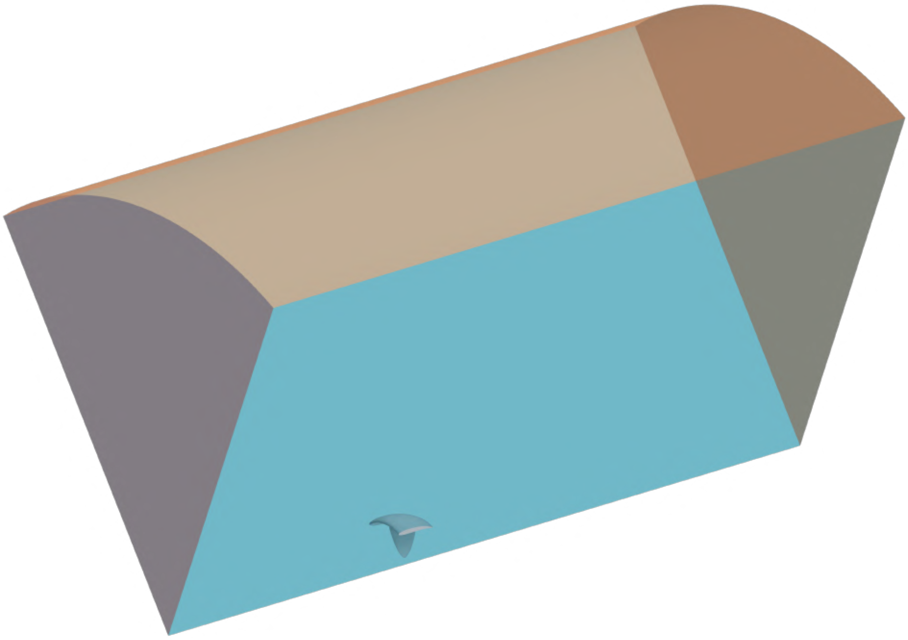

Fig. 4: Computational domain of steady simulations.

2.3 Mesh analysis

The thruster performances are typically expressed by thrust and torque coefficients and the open water efficiency η_0. In RDT we define those coefficients including not only the propeller forces and torque but also the rim ones generated by rim and duct. In particular we define:

$$K_t = \frac{T_{propeller} + T_{duct} + T_{rim}}{\rho n^2 D^4} \quad (1)$$

$$K_q = \frac{Q_{propeller} + Q_{rim}}{\rho n^2 D^5} \quad (2)$$

$$\eta_0 = \frac{J}{2\pi} \frac{K_t}{K_q} \quad (3)$$

where $J = V_a/nD$ is the commonly defined advance coefficient.

The mesh used for geometrically non-resolved gap RANS simulations is made following the guidelines consolidated in Gaggero and Villa (2018), obtaining an average of 1.3 million cells. Of course, keeping the same mesh parameters but including the gap geometry, the number of cells in the gap resolved simulation increases. In order to determine the number of cells needed to capture the relevant gap fluid dynamic effect, starting using the same mesh parameters of the non-resolved gap, a convergence analysis by changing only the number of added cells in the gap was conducted. The gap geometry used for this analysis is the reference one obtained with the parameters in Tab. 2.

Table 2: Initial gap geometry parameters

ID	w [mm]	d [mm]	t [mm]	α_1 [°]	α_2 [°]
0/0	40	5	1	0	0

Note that, to quickly refer to the different parametric configurations of the gap geometry, the nomenclature: (α_1/α_2) is used. In these cases, where not otherwise specified, it means that all other geometric characteristics are kept equal to the reference values reported in table 2.

Table 3 shows, in terms of KT, the results of this analysis, conducted using the procedure proposed in Eça and Hoekstra (2014), which indicate the need of adding about 300 000 cells to achieve an uncertainty and an error respectively less than 2% and 1%.

Table 3: Mesh convergence analysis in DRD gap-resolved simulations, K_t values normalized with respect to modeled-gap performances for confidentiality reasons

cells	$K_t/K_{t_{ref}}$	uncertainty [%]	extrapolated error [%]
1 371 102	0.9715	2.0	0.68
1 565 886	**0.9703**	**1.9**	**0.55**
3 243 345	0.9669	1.3	0.22
10 542 940	0.9665	0.6	0.17

This increment of about 15% in the cells number with respect to the non-resolved gap mesh, produces a calculation grid with approximately 1.6 million cells. A typical example of such mesh is shown in figure 5.

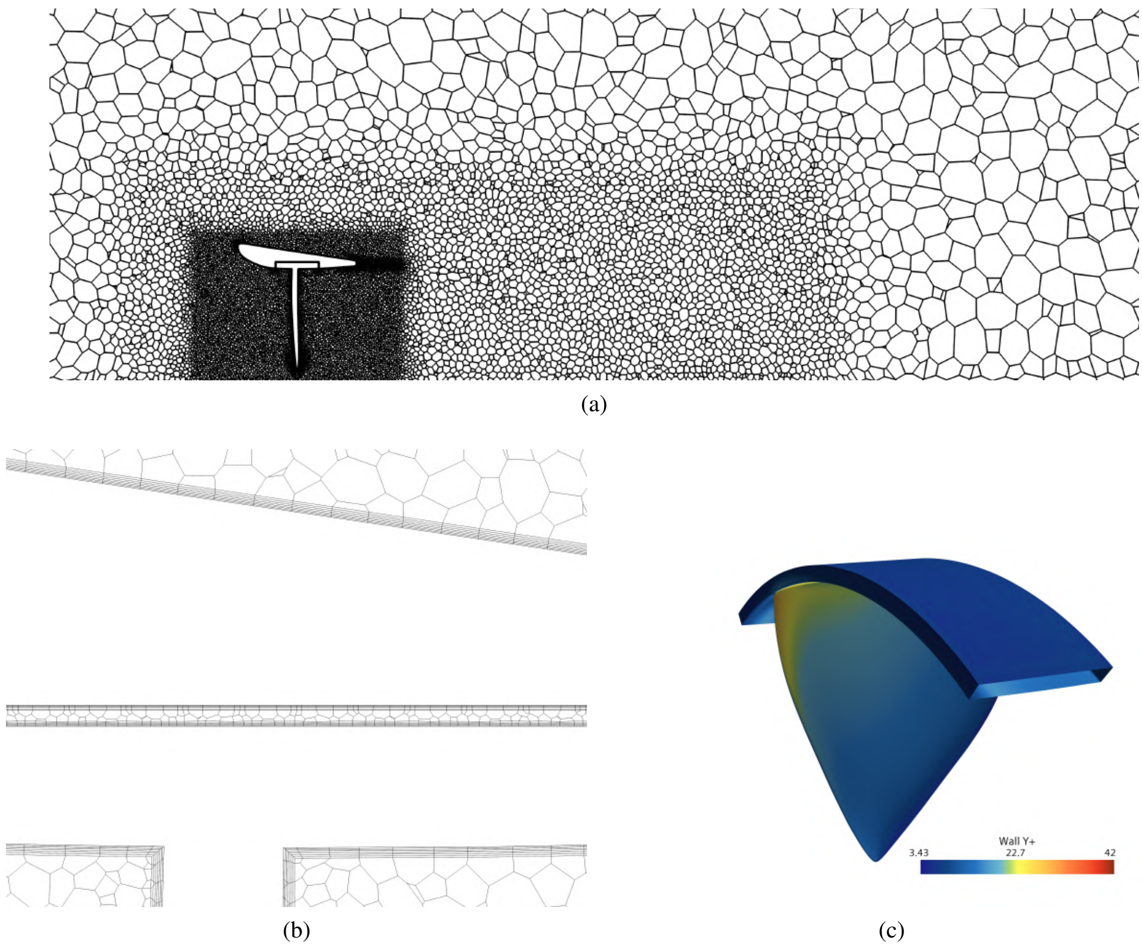

Fig. 5: Typical mesh of gap-resolved, steady simulations (a) with gap mesh detail (b) and $y+$ values in gap and blade (c).

Furthermore, an analysis was conducted on the mesh of the boundary layer inside the gap. In fact, while for the external flow the parameters already validated by Gaggero and Villa (2018) were used, for the flow inside the gap, due to the different geometric and characteristic velocity scales, it was necessary to investigate the size of the cells necessary to correctly capture the effects in the boundary layer. The first guess of thickness was obtained using the relations for turbulent boundary layer (Schlichting (1979)) where was used the Reynolds number defined as:

$$Re = \frac{tnD/2}{\nu} \tag{4}$$

Using the simulations results, the first guess thickness was corrected to obtain a gap $y+$ distribution in line with the values already used in similar works (Zhai et al. (2022)). In particular, the $y+$ distribution shown in figure 5c was obtained, where $y+_{max \simeq 17}$.

3 Results and discussion

The first analysis conducted concerns the comparison between the performances of the RDT in both CRD and DRD configurations, obtained using a mesh with and without a geometrically resolved gap. These simulations were carried out on the reference geometry of the gap whose characteristics are shown in table 2, i.e. rim thickness $d = 5\,mm$, gap thickness $t = 1\,mm$, rim width $w = 40\,mm$, and front and rear angles equal to $\alpha_1 = \alpha_2 = 0°$. Furthermore, on these geometries, to verify that the modeling hypotheses provided acceptable results, unsteady analysis without exploiting the periodicity of the problem were also conducted. The results of this analysis are presented in 4 in terms of K_t, K_q and η_0. Note that for confidentiality reasons the values relating to the DRD have been normalized with respect to modeled-gap performances.

Table 4: Results in standard (0/0) configurations, DRD values normalized with respect to modeled-gap performances for confidentiality reasons.

Case	J	K_t	K_q	η_0
CRD w/o gap	0.7	0.4296	0.0854	0.5603
CRD with gap	0.7	0.4221	0.0881	0.5340
CRD Unsteady with gap	0.7	0.4217	0.0887	0.5296
Case	J/J_{ref}	$K_t/K_{t_{ref}}$	$K_q/K_{q_{ref}}$	η_0
DRD w/o gap	1	1	1	0.5850
DRD with gap	1	0.9703	0.9911	0.5730
DRD Unsteady with gap	1	0.9619	0.9852	0.5716

First of all we noted that the error on performance between gap resolved steady state simulation using periodic BC and MRF and the unsteady ones, extracted as the mean of the last propeller revolution, is less than 1% so it's confirmed that the assumptions adopted in simplified model are accurate enough to correctly solve the physics of the problem. Moreover, from the results obtained we note that the efficiency loss due to the gap is much higher in the CRD case compared to the DRD. This aspect can be explained by physically analyzing the gap effect. Mainly, the loss of efficiency due to the gap is due to two distinct phenomena. The first is the increase in torque compared to the case without gap due to the fact that an extra face is added in contact with the water and therefore a bigger wet surface causing friction is considered. This component is present in both RDT configurations substantially in the same way. Note that this effect is not exactly the same in the two configurations due to the fact that it is slightly influenced by the pressure field. In fact, depending on the pressure difference downstream and upstream of the gap, an axial flow opposite to the direction of the inflow develops within the gap. This axial flow, as highlighted by various works on the Taylor-Couette flow (Hwang (2004)), influences and, in particular, reduces the torque necessary to rotate the rim. Moreover, the effect of the increase in torque due to friction is not directly observable from the K_q values. These, in fact, also contain the contribution of the propeller blades and, consequently, are influenced by the modification of the driving torque on the blade due to the modification of the pressure field induced by the propeller and the duct. In fact, while in the CRD case we notice an increase in torque in the case of a resolved gap compared to the modeled-gap case, in the DRD we notice the opposite. It is important to note that this effect on the pressure field due to the gap is in the cases analyzed more relevant than the friction contribution due to the increase in the wetted surface and is strongly dependent not only on the geometry of the gap, but also, on the pressure field developed by the propeller and duct. The gap, in fact, puts the pressure and the suction sides of the blade in “communication”, near the tip of the blade which, in the RD configuration is a loaded area. It is therefore clear that the higher the pressure difference across the blades, the greater the effect of the gap will be in “restoring” it. Considering the pressure fields of the two configurations shown, in terms of $C_{PN} = \frac{2P}{\rho n^2 D^2}$, in figure 6 we note that in the case of CRD the pressure difference is much higher than in the DRD case. In fact, despite pressure, as expected, is overall higher in divergent configuration, we note that across propeller blade there is a C_{PN} jump of about 1.42 in the convergent case while in the divergent this value is about 0.95.

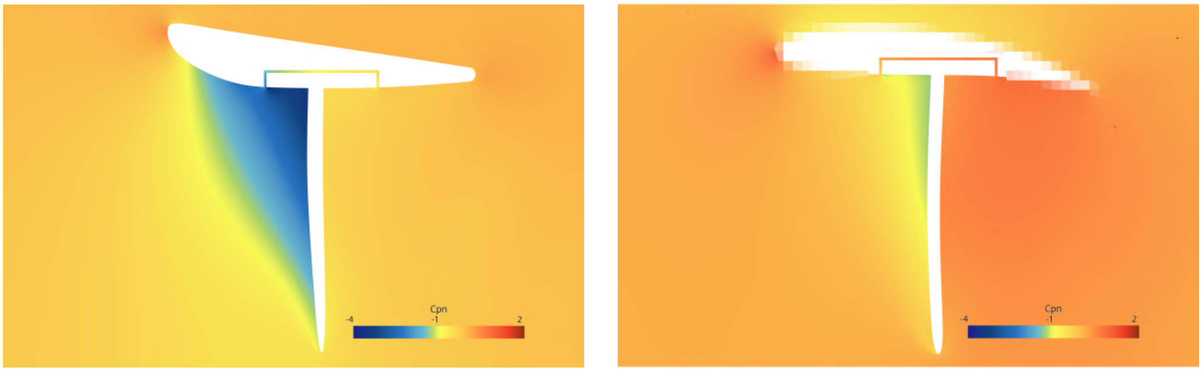

(a) (b)

Fig. 6: Pressure coefficient (C_{PN}) field in CRD (a) and DRD (b) configurations. DRD duct geometry hidden for confidentiality reasons

This pressure jump causes an axial velocity component to develop inside the gap which adds to the rotational one caused by the friction with the rim. A typical gap flow is shown in figure 7b. Due to the fact that the pressure is higer in the pressure side with respect to the suction side of the propeller blade, the axial component has a direction opposite to the main flow. For this reason, considering the inflow as x-direction, in the gap the x-component of the velocity is negative. In the analyzed cases this velocity has the profile shown in figure 7a. We note that given the greater driven pressure gradient in the CRD case, the maximum axial speed reached is about -1.5 m/s and the flow rate approximately 0.7 kg/s while in the DRD case the maximum speed is approximately -1.2 m/s and the flow rate near 0.42 kg/s

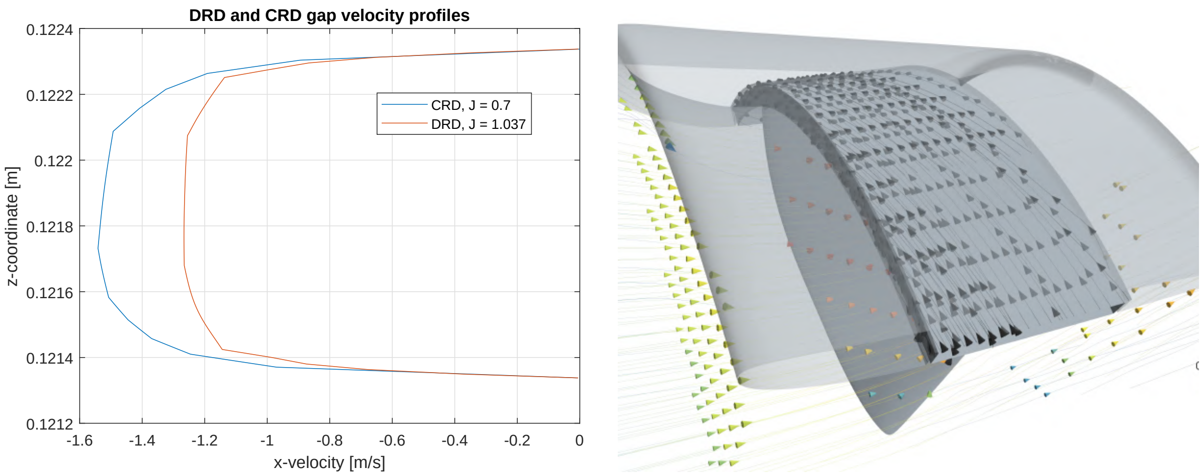

(a) (b)

Fig. 7: Gap x-velocity profile in CRD and DRD thruster (a) and typical gap flow (b).

Despite that, the contribution given by the interaction between the pressure field and flow in the gap is not immediately and generically understandable. In fact, with what has been stated above, one could expect that the effect of the gap due to the pressure delta between the face side and the suction side is to reduce the thrust compared to the case without the gap and that consequently the greater the pressure difference, the greater the loss of thrust due in the presence of the gap. In reality the numbers obtained deny this interpretation. In fact, although there is a decrease in both the DRD and CRD configurations of the thrust due to the presence of the gap, the entity of this reduction is equal to approximately 1.5% in the CRD case (greater ΔC_{PN}) while it is approximately 2.5% in the DRD case (smaller ΔC_{PN}). On the other hand, the increase in parasitic torque due to the gap is approximately 3% in the CRD case, while in the DRD case it is almost -1%. This means that the effect of the gap in the DRD configuration is to reduce the driving torque of the propeller compared to the case without the gap resolved. In other words, the variation in the pressure field induced by the gap unload the propeller blade near the tip causing both a reduction in thrust and in torque. In any case, the effect of the gap also in the DRD case leads to a decrease in efficiency since the loss of thrust is greater than the reduction in torque. It appears clear from these considerations that the effect of the gap on the propeller performance is not trivial and strongly depends on the pressure field generated by both the blade and duct.

After having analyzed the impact of the gap on the flow and performance of the RDTs, parametric analyzes were carried out on the geometric characteristics of the gap itself to better understand how, individually, these were linked to the loss of efficiency of the thruster. Two families of analyzes were conducted: the first to understand the effect of the gap thickness and the second to determine the influence of the gap shape. The first parametric analysis, in particular, has been conducted varying the gap thickness while keeping the other geometric characteristics constant and equal to the reference ones. The performance of the RDT was evaluated in both CRD and DRD configurations for gap thicknesses varying from 0.5 to 1.5 mm. The results of the analysis conducted are presented in table 5.

Table 5: Gap thickness effect on RDT performances. DRD values normalized with respect to modeled-gap performances for confidentiality reasons.

DRD thruster, $J/J_{rif} = 1$					CRD thruster, J = 0.7			
t [mm]	$K_t/K_{t_{ref}}$	$K_q/K_{q_{ref}}$	η_0		t [mm]	K_t	K_q	η_0
1.5	0.9511	0.9823	0.5664		1.5	0.4167	0.0878	0.5287
1.2	0.9609	0.9867	0.5697		1.2	0.4201	0.0881	0.5312
1.0	0.9703	0.9911	0.5730		1.0	0.4221	0.0881	0.5340
0.8	0.9711	0.9926	0.5723		0.8	0.4243	0.0881	0.5366
0.5	0.9805	0.9955	0.5762		0.5	0.4278	0.0885	0.5385

The results obtained indicate that the greater the thickness of the gap, the lower the efficiency of the thruster and so that is appropriate to minimize the thickness of the gap. These results foster the assumption previously mentioned, on the phisical effect of the gap and are valid in the range of thicknesses reported in table 5 but it has been verified that by further reducing the thickness of the gap a point is reached where, due to the viscous effects and the increase of viscous shear stress in gap, the torque increases significantly causing a loss of efficiency. However, this effect occurs using gap thickness values that are not technologically achievable and are therefore not of interest. In fact, although the technologically achievable gap value does not depends directly to the diameter, for standard blade, the minimum gap reference values are between 0.5% and 1% of D, which in the analyzed configurations correspond to 1.1 - 2.3 mm.

The second parametric analysis conducted concerns the shape of the gap. In particular, keeping the thickness $t = 1\,mm$ fixed and the blade-side rim width $w = 40\,mm$, the front and rear angles were varied in a range from -60° and 60° with 15° step. Naturally, since the rim width w is kept constant in order to contain the blade root, varying the angles causes a variation in the width of the duct-side of the gap l. The results in terms of efficiency of the analysis for both the CRD and the DRD are shown in the figure

8.

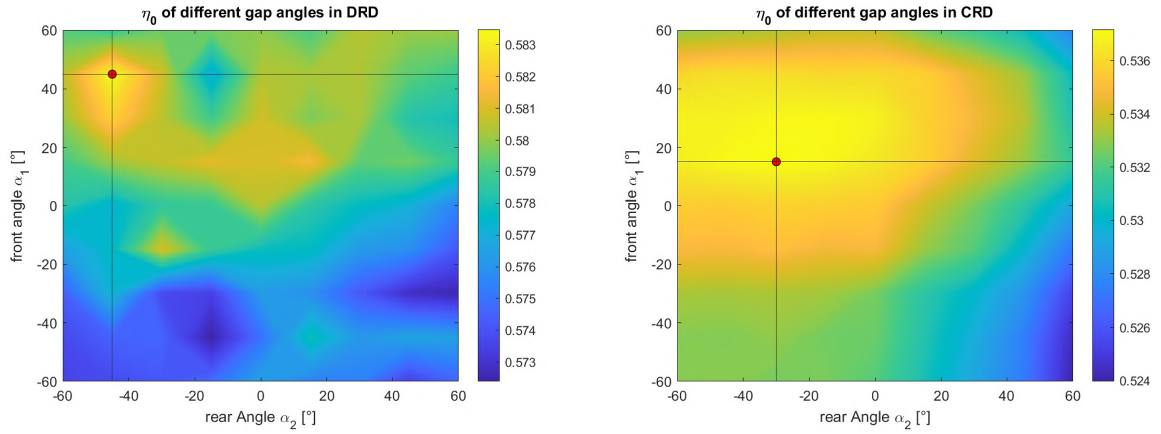

(a) optimal: $\alpha_1 = 45°$, $\alpha_2 = -45°$ (b) optimal: $\alpha_1 = 15°$, $\alpha_2 = -30°$

Fig. 8: Open water efficiency vs front (α_1) and rear (α_2) angles in DRD (a) and CRD (b) configurations.

From the analysis of CRD geometries it emerges that the optimum is obtained in the (15/-30) configuration whose pressure field, in terms of pressure coefficient C_{PN}, is shown in figure 9a.

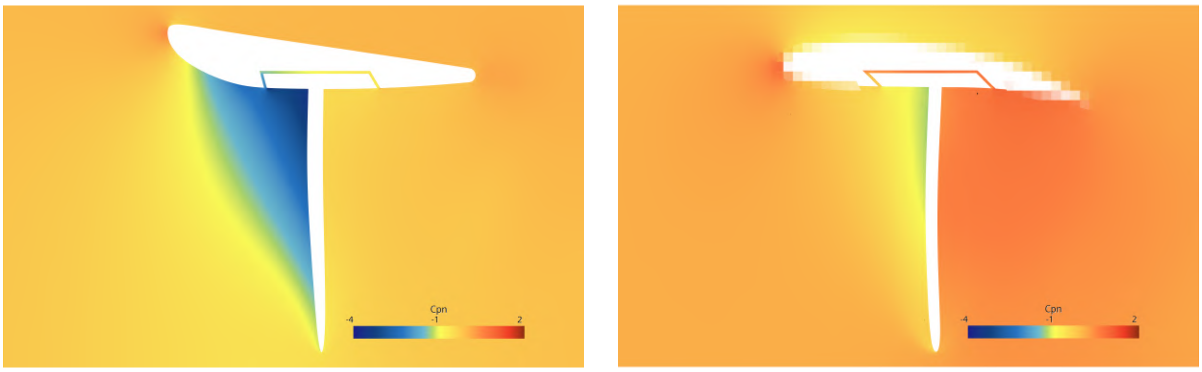

(a) optimal: $\alpha_1 = 15°$, $\alpha_2 = -30°$ (b) optimal: $\alpha_1 = 45°$, $\alpha_2 = -45°$

Fig. 9: Pressure coefficient (C_{PN}) fields in optimal CRD (a) and DRD (b) configurations. DRD duct geometry hidden for confidentiality reasons

In this case we note that the inner gap length l is not the minimum that would be obtained in the (60/-60) configuration and that therefore minimizing the wetted surface is not always the best solution. The contribution of pressure, in fact, has generally a great influence on the RDTs performances. For example in the optimal case the inner gap surface torque is greater than in the (60/-60) configuration of about 40%. However in the optimal configuration the pressure field is such that the torque required from the blade and the rim surface in contact with the blade is smaller with respect to the 60/-60 configuration. Overall the pressure effect on the blade is greater than the torque increment due the increase in wetted surface. This effect is even more evident in the optimal DRD configuration whose pressure field, in terms of pressure coefficient (C_{PN}), is shown in figure 9b where the duct geometry has been hidden for confidentiality reasons. In the DRD case, as shown in figure 8a, the efficiency is much more irregular and presents a fairly clear peak in the (-45/45) configuration. In any case the effect of the gap remains not trivial, in fact there is not a direct correlation between gap ΔC_{PN} or gap-flow speed and the loose in efficiency. This is due to the fact that there are two opposite effects: on one side the axial velocity in the gap reduce the required driving torque as documented in studies on the Taylor-Couette flow (Hwang (2004)), on the other the greater the velocity and the mass flow in the gap, the greater the induced variation in the pressure field across the blade and so a change in blade torque and thrust. It is not therefore possible to generalize the gap effect but is necessary to consider the interaction between the gap flow and the specific duct and the propeller geometries in the working point conditions.

Figure 10 shows the results of the analysis of the gap effect as the operating point varies. In both the CRD and DRD cases we note from the open water diagrams obtained that the effect of the gap is substantially a constant offset in performance, manily due to the variation of the torque. In the DRD configuration we notice that there is a slight decrease on the gap effect at high advance coefficients ($J/J_{ref} \simeq 1.25$). However, given the small extent of this effect, it can be concluded that the gap effect does not vary substantially if the engine finds itself working in a condition different from the design one for any reason during its operational life.

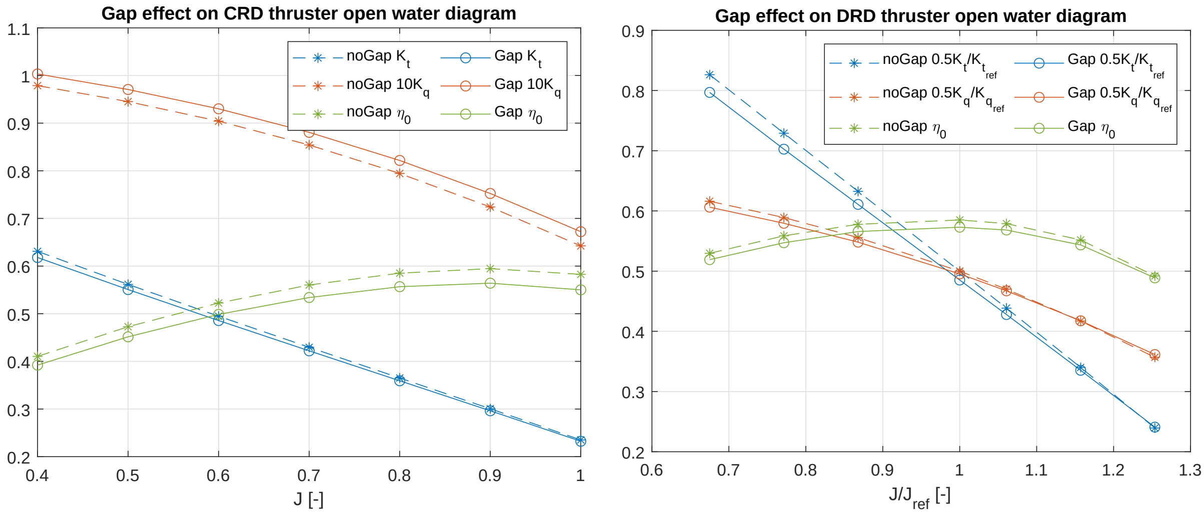

(a) (b)

Fig. 10: Gap effect on RDT open water diagram in CRD (a) and DRD (b) configurations.

4 Conclusions and future work

Several simulations have been carried out in order to better understand the effects of the gap in both convergent and divergent RDT thrusters. It was found that the effect of the gap on the propulsive efficiency is more marked in convergent configurations while it is substantially negligible in divergent ones. Moreover, by carrying out convergence analyzes on the meshes, it was noted that to correctly resolve the gap effects it is necessary to increase the size of the calculation grid by 15-20%. By exploiting the periodicity of the problem and using stationary MRF simulations it is therefore possible to perform simulations on RDTs with a gap resolved with a mesh of approximately 1.6 million cells while maintaining the thrust error within approximately 2%.

As far as the geometry of the gap is concerned, it has been noted that the thickness has a negative influence, and it is therefore advisable to limit it to the minimum possible while the angles (shape) of the gap do not have an obvious optimal configuration. Certainly, as already confirmed by the literature, reducing l reduces the added torque due to the friction of the rim in the gap. However, also considering the effect of the pressure field, it is not certain, and indeed in the cases analyzed it was not the case, that the configuration with minimum l is the one with the highest efficiency.

In conclusion, therefore, considering the relatively small increase in computational cost and the difficulties in generalizing the gap effect as it is strongly dependent on the pressure field and therefore on the duct and propeller geometries, it is believed that for future work it is preferable to investigate the RDTs by including the gap in the simulations geometry.

Acknowledgements

This work has been partially supported by Spoke 3 "Waterways" within the Italian PNRR National Centre for Sustainable Mobility (MOST) funded by the European Union - NextGenerationEU. Opinions expressed are those of the authors only and do not necessarily reflect those of the European Union or the European Commission. Neither the European Union nor the European Commission can be held responsible for them.

References

Y. Su, J. Lin, D. Zhao, C. Guo, C. Wang and H. Guo (2020). Real-time prediction of large scale ship model vertical acceleration based on recurrent neural network. *Journal of Marine Science and Engineering*, **8**(10), 777.

H. Grümmer (2016). Design and Optimization of a Hubless rim-driven Thruster for an Autonomous Surface Vehicle using RANSE Simulation. *Doctoral dissertation, MS Dissertation, Department of Dynamics of Maritime Systems, Technical University of Berlin, German*.

X. Yan, X. Liang, W. Ouyang, Z. Liu, B. Liu and J. Lan (2017). A review of progress and applications of ship shaft-less rim-driven thrusters. *Ocean Engineering*, **144**, 142?156.

C. Pashias and S. R. Turnock (2003). Hydrodynamic design of a bi-directional, rim-driven ducted thruster suitable for underwater vehicles. *Ocean Engineering*, **144**, 142?156.

S. A. Kinnas, S. H. Chang, L. He and J. T. Johannessen (2009). Performance prediction of a cavitating RIM driven tunnel thruster. *In First International Symposium on Marine Propulsors SMP*, **Vol. 9**, 435-442.

B. W. Song, Y. J. Wang and W. L. Tian (2015). Open water performance comparison between hub-type and hubless rim driven thrusters based on CFD method. *Ocean Engineering*, **103**, 55-63.

Q. M. Cao, F. W. Hong, D. H. Tang , F. L. Hu and L. Z. Lu (2012). Prediction of loading distribution and hydrodynamic measurements for propeller blades in a rim driven thruster. *Journal of Hydrodynamics*, **24**, 50-57.

A. J. Dubas, N. W. Bressloff and S. M. Sharkh (2015). Numerical modelling of rotor?stator interaction in rim driven thrusters. *Ocean engineering*, **106**, 281-288.

M. Lea, D. Thompson, B. Blarcom, J. Eaton, J. Friesch and J. Richards (2003). Scale model testing of a commercial rim-driven propulsor pod. *Journal of ship production*, **19**(02), 121-130.

B. Liu, M. Vanierschot and F. Buysschaert (2022). Effects of transition turbulence modeling on the hydrodynamic performance prediction of a rim-driven thruster under different duct designs. *Ocean Engineering*, **256**, 111-142.

A. W. Hughes, S. A. Sharkh and S. R. Turnock (2000). Design and testing of a novel electromagnetic tip-driven thruster. In ISOPE International Ocean and Polar Engineering Conference (pp. ISOPE-I). ISOPE.

S. M. Abu Sharkh, S. R. Turnock and G. Draper (2000). Performance of a tip-driven electric thruster for unmanned underwater vehicles. In ISOPE International Ocean and Polar Engineering Conference (pp. ISOPE-I). ISOPE.

B. Liu and M. Vanierschot (2021). Numerical study of the hydrodynamic characteristics comparison between a ducted propeller and a rim-driven thruster. *Applied Sciences*, **11**(11), 4919.

H. Jiang, W. Ouyang, C. Sheng, J. Lan and R. Bucknall (2022). Numerical investigation on hydrodynamic performance of a novel shaftless rim-driven counter-rotating thruster considering gap fluid. *Applied Ocean Research*, **118**, 102967.

B. Liu, M. Vanierschot and F. Buysschaert (2023). Optimization design of the duct of a rim-driven thruster using the adjoint approach. *Ocean Engineering*, **278**, 114293.

L. Peng, Y. Hua-Dong, W. Chao and W. Kaiqiang (2023). Improved efficiency with concave cavities on S3 surface of a rim-driven thruster. *Physics of Fluids*, **35**(10), 107102.

Q. Cao, X. Wei, D. Tang and F. Hong (2014). Study of gap flow effects on performance of rim driver thrusters. In Proceedings of the 13th National Conference on Hydrodynamics and the 26th National Symposium on Hydrodynamics, Tsingtao, China, 1197-1206.

J. Lin, H. D. Yao, C. Wang, Y. Su and C. Yang (2023). Hydrodynamic performance of a rim-driven thruster improved with gap geometry adjustment. *Engineering Applications of Computational Fluid Mechanics*, **17**(1), 2183902.

S. Gaggero (2023). Numerical design of a RIM-driven thruster using a RANS-based optimization approach. *Applied Ocean Research*, **94**, 101941.

S. Gaggero, M. Viviani, G. Tani, F. Conti, P. Becchi and F. Valdenazzi (2013). Comparison of different approaches for the design and analysis of ducted propellers. In proceedings of the V International Conference on Computational Methods in Marine Engineering.

S. Gaggero (2020). RIM driven propellers design using a Simulation Based Design Optimization approach. In proceedings of the 5th International Conference on Maritime Technology and Engineering - MARTECH. Lisbon.

S. Gaggero and D. Villa (2018). Cavitating propeller performance in inclined shaft conditions with openfoam: Pptc 2015 test case. *Journal of Marine Science and Application*, **17**(1), 1-20.

L. Kort (1940). Elektrisch angertriebene schiffsschraube. German Patent, 688 (1940), p. 13.

L. Eça and M. Hoekstra (2014). A procedure for the estimation of the numerical uncertainty of CFD calculations based on grid refinement studies. *Journal of Computational Physics*, **262**, 104-130.

J. Y. Hwang and K. S. Yang (2004). Numerical study of Taylor–Couette flow with an axial flow. *Computers & Fluids*, **33**, 97-118.

Siemens Digital Industries Software, (2021). Simcenter STAR-CCM+, version 2021.2.1.

S. Zhai, S. Jin, J. Chen, Z. Liu and X. Song (2022). CFD-based multi-objective optimization of the duct for a rim-driven thruster. *Ocean Engineering*, **264**, 112467.

H. Schlichting (1979). *Boundary Layer Theory.* 7th Edition, McGraw-Hill, New York.